Corrosion Science 198 (2022) 110113

Contents lists available at ScienceDirect

Corrosion Science

journal homepage: www.elsevier.com/locate/corsci

The effect of salt composition on the stress-free and corrosion-fatigue performance of a fine-grained nickel-based superalloy

M.L. Hendery [a,b,*], M.T. Whittaker [a], B.J. Cockings [a], P.M. Mignanelli [b]

[a] Institute of Structural Materials, Swansea University, Swansea SA1 8EN, United Kingdom
[b] Rolls-Royce plc, Derby, United Kingdom

ARTICLE INFO

Keywords:
Molten salts
Nickel
Superalloys
Corrosion fatigue
Sulphidation

ABSTRACT

This paper describes work to study hot corrosion damage in the nickel-based gas turbine alloy RR1000 coated with various salts at 600 °C. Interest in type-II hot corrosion on the fatigue resistance of gas turbine alloys has increased to minimise power/thermal inefficiencies. Stress-free corrosion demonstrated a greater impact of sulphate (versus chloride) on maximum pit depth, a key influencing factor of fatigue lives. In corrosion-fatigue testing, at low stresses sulphate was shown to be more influential of fatigue life. At high stresses, the presence of greater crack initiation sites, reduced initiation lives and cracked oxide suggests chlorine influenced the crack-initiation behaviour.

1. Introduction

Gas turbine engines used in modern civil aerospace operations necessitate the use of high-temperature materials in order to optimise the thrust and fuel efficiency. Nickel-based superalloys are often used in the compressor and turbine components due to their resistance to creep, fatigue and harsh corrosive environments, even at temperatures as high as 1050 °C [1].

With the ever increasing demand for the reduction of emissions and lifecycle costs in the civil aerospace industry, modern gas turbines are being driven harder to generate higher pressure ratios [2]. As a result, rotors need to cope with the increase in turbine entry temperature (TET) and associated temperatures of the compressor and turbine sections. When combined with the high stresses encountered in rotors, a significant demand is placed on these high-strength nickel-based superalloys. Gas turbine rotors are exposed to a harsh combustion environment; sodium-based salts ingested from the atmosphere in coastal and desert areas, and sulphur dioxide bearing combustion and exhaust gases [3].

Environmental damage has a significant impact on the fatigue behaviour of nickel-based alloys through oxidation and hot corrosion. Two principle types of hot corrosion are discussed in the literature: types I and II. Type I corrosion is restricted to high temperatures (above 900 °C) since the oxide ions which need to be produced are kinetically constrained at lower temperatures. It is therefore common to separate Type I hot corrosion into two stages: a low corrosion rate incubation period followed by accelerated corrosion attack [4]. During the incubation period the initial protective and non-protective oxides (Al_2O_3, Cr_2O_3, CoO and NiO) are formed. The initiation of the accelerated corrosion attack is thought to be due to the breakdown of these oxides via salt fluxing models. The formation of NiO on the alloy surface produces an oxygen gradient across the salt layers (such as Na_2SO_4) that are deposited onto the material. Sulphur then diffuses and enters the base metal forming $NiSO_4$ with the resulting NiO_2^{2-} ions diffusing to the salt-gas interface where they decompose to NiO particles and ions. As the salt is consumed sulphur no longer enters the alloy and prevents the formation of oxide ions. Here the acceleration of oxidation begins. Once the salt layer is fully saturated with nickel, a continuous NiO layer forms adjacent to the NiS layer, thereby preventing further accelerated oxidation [5]. The end result is a porous outer oxide scale with internal sulphides in the alloy substrate [6].

Type II corrosion typically occurs at lower temperatures (650–750 °C) due to the formation of sulphates ($NiSO_4$, $CoSO_4$), which require higher SO_3 partial pressures that are not usually found at higher temperatures. This form of attack usually generates pitting damage with little internal sulphidation of the alloy substrate.

It is generally accepted that a liquid film is required for hot corrosion and that dissolution of non-protective metal oxides MO (where M is represented by Co and Ni for RR1000) takes place at the salt-oxide interface. Once the salt is saturated the M ions migrate through the liquid film and precipitate as MSO_4 dependant on temperature and SO_3

* Corresponding author at: Institute of Structural Materials, Swansea University, Swansea, SA1 8EN, United Kingdom.
E-mail address: mathew.hendery@rolls-royce.com (M.L. Hendery).

https://doi.org/10.1016/j.corsci.2022.110113
Received 9 October 2021; Received in revised form 10 January 2022; Accepted 19 January 2022
Available online 22 January 2022

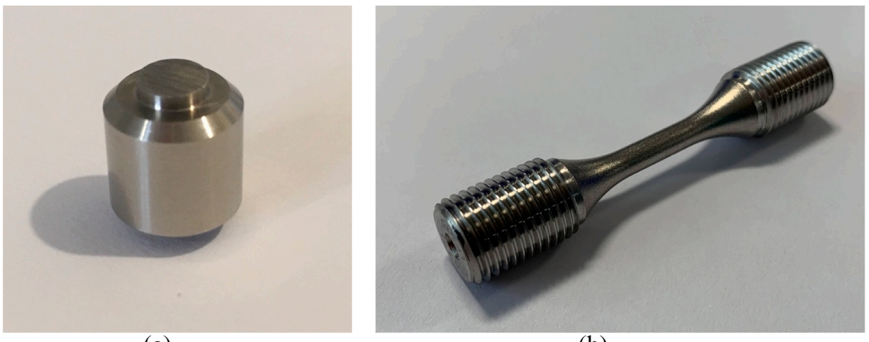

(a) (b)

Fig. 1. (a) Left: Round bobbin specimen used for stress-free hot corrosion trials. (b) Right: Fatigue specimen used in corrosion-fatigue trials.

partial pressure. The overall corrosion rate is therefore proportional to two factors: the rate of non-protective oxide dissolution and the rate of protective oxide formation. A continuous protective oxide layer forms more readily at higher temperatures and therefore corrosion rates decrease, with a maximum rate of corrosion in the 600–800 °C region [7].

The three salts used in this study (two of which were down-selected for corrosion-fatigue trials) consider the effects of varying the type of sulphates, chlorides, and their proportions. Investigation into potassium-based salts has been limited and mostly focussed on its effect on steel alloys, at elevated temperatures or on stress-free specimens [8–10]. The potential effect of K_2SO_4 on type II hot corrosion has been previously investigated in coal combustion systems as a theoretical exercise and the generation of a low temperature melting eutectic with $CoSO_4$ discussed [7]. The effect of chlorine content on the hot corrosion of Ni-based alloys has had slightly more focus than potassium-based salts; Encinas-Oropesa et al. [3] varied the proportion of NaCl in the salt applied to RR1000, alloy720LI and Waspaloy and observed that a reduction in chlorine resulted in greater corrosion damage at 700°C.

Historically corrosion-fatigue assessments involved the pre-corrosion of fatigue samples in corrosive environments [11–14], prior to air-fatigue testing at elevated temperatures. Whilst these demonstrated life-debits, the corrosion mechanisms can be more accurately investigated through the application of salt and subsequent application of cyclic load in a corrosive gaseous environment [15,16]. Pedrazzini et al. [17] considered the influence of 98%Na_2SO_4-2%NaCl and an SO_2 environment on the dwell fatigue performance of RR1000, which demonstrated a reduction in fatigue life and enhanced crack growth rates compared to air-only fatigue. Finally, Child et al. [15] showed that altering the applied salt flux (salt quantity) greatly influenced the crack initiation behaviour and resultant fatigue life of RR1000 at 700 °C. The study also showed that at lower applied stresses, corrosion occurred through a mixed-oxide scale formation and spallation.

In the present study, fine grain (FG) RR1000 was subjected to type II hot corrosion under both stress-free and corrosion-fatigue conditions. This article represents the first instance of the effect of salt composition on the type II hot corrosion of a Ni-based superalloy at 600 °C and provides a new insight into the effects of chloride and sulphate-based species.

2. Experimental methods

RR1000 is a γ' precipitation hardened nickel-based alloy used for gas turbine rotors at temperatures up to 725 °C [18]. Round bobbin RR1000 specimens for stress-free corrosion testing, Fig. 1a, were machined from a fully heat treated fine grain (FG) forging with an average grain size of 4–8 μm [19]. Plain cylindrical fatigue specimens, Fig. 1b, were also machined from the RR1000 forging. The specimen design was of a cylindrical round bar of ø4.5 mm and 15 mm gauge length. The specimen surfaces were machined to a specification of $R_a < 0.25$ μm prior to shot peening using 110H steel cast shot, to a specification of 6–8 Almen intensity and 200% coverage. An electro-chemically etched sample of FG RR1000 shows the distribution of γ' precipitates around a γ matrix in Fig. 2. The etchant used was 10% oxalic acid with a voltage of 6 V for 3 s.

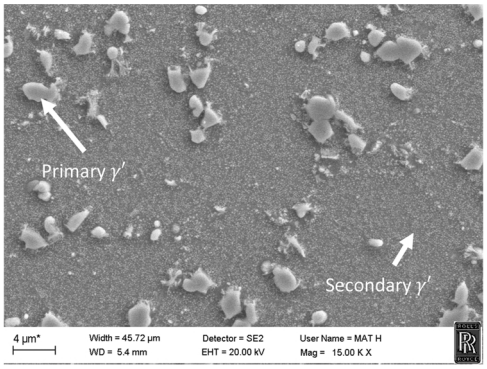

Fig. 2. FG RR1000 electro-chemically etched with 10% oxalic acid at 6 V for 3 s. The etchant removed the γ matrix, leaving the γ' precipitates.

The salting procedure for both series of trials pre-heated the specimens to a temperature of 105 °C on a hot plate before moving to a stationary mount or turntable (for bobbins and fatigue samples respectively) and the salt applied using a spray gun connected to a pressurised air source. The use of a variable aperture spray gun and an automated, timed hydraulic actuator allows consistent salt application and the ability to replicate the technique with a high degree of repeatability. The fatigue specimens were weighed pre- and post-salting in order to ensure correct salt loading. A standard salt loading level of 0.138 mg/cm^2 was chosen to generate pitting type damage rather than broad front material loss [20,21].

A three-zone furnace surrounding a central gas tight chamber containing a gaseous corrosive environment was used for the stress-free corrosion testing. The test chamber was purged with an inert atmosphere during heating and cooling. The corrosive environment used was a pre-mixed air-300 ppm SO_2 gas under continuous flow. Schematics for both the stress-free and corrosion-fatigue experimental setups are given in Fig. 3.

Load controlled low cycle fatigue (LCF) testing was conducted at 600 °C and at a stress range to induce failure between 10^3 and 10^5 cycles using a fully reversed ($R = -1$) waveform over a 6 s triangular waveform (i.e., frequency = 0.16667 Hz). Complete specimen rupture or run out (10^5 cycles) were chosen as the test end criteria. The same environments and procedures were used in LCF testing as those in the stress-free testing.

Stress-free corrosion data was obtained for non-shot peened specimens coated with one of three salts: 55%K_2SO_4-45%KCl, 98%Na_2SO_4-

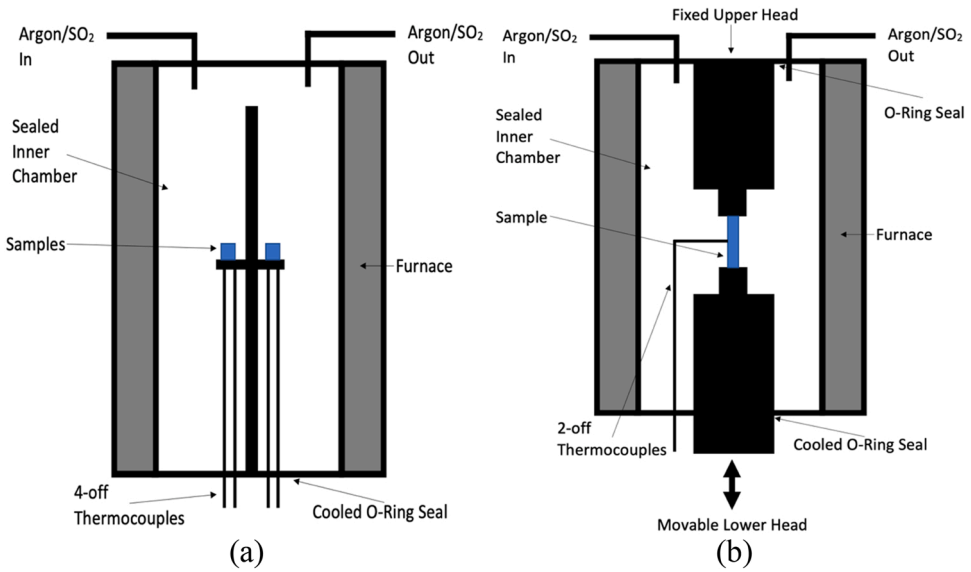

Fig. 3. (a) Left: Schematic of the stress-free corrosion environment. (b) Right: Schematic of the load controlled corrosion-fatigue environment used.

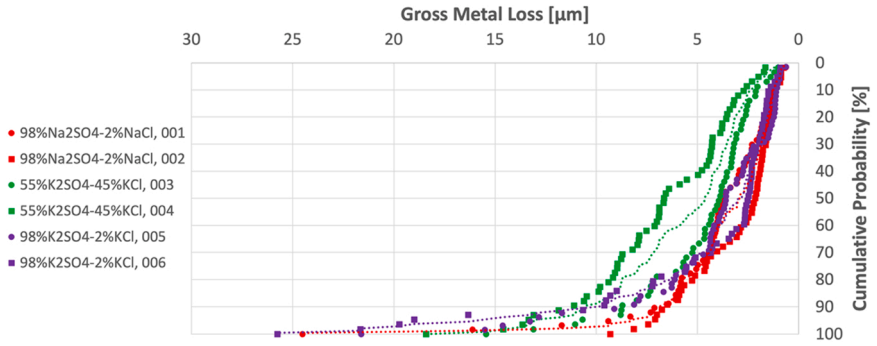

Fig. 4. Variation in metal loss (pit depth) for FG RR1000 after exposures of 50 h in an air-300 ppm SO2 environment at 600 °C with varying salt composition.

2%NaCl and 98%K_2SO_4-2%KCl. This data was generated to supplement a previous series of testing [22]. Fatigue data was generated for shot peened specimens coated with two of these salts; 55%K_2SO_4-45%KCl and 98%Na_2SO_4-2%NaCl.

Post exposure and testing, the fatigue specimens were stripped of oxide by soaking in an alkaline cleaning solution of Ardrox 1435b solution (30% concentration) at room temperature for a period of 4 h in an ultrasonic bath, followed by a rinse with flowing distilled water. This was conducted to allow surface profilometry of the gauge length to obtain pit depth data. Additional cross-sections of the fatigue samples were imaged and both methods of metal loss measurement compared.

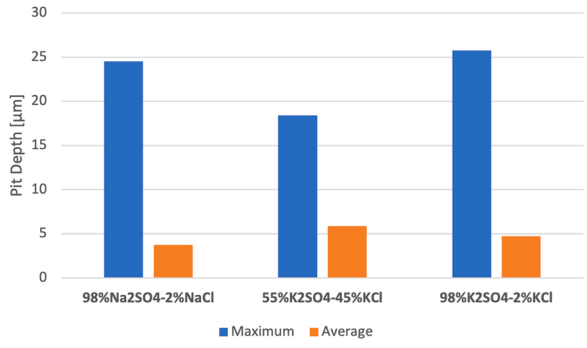

Fig. 5. Mean and maximum gross metal loss (pit depths) for FG RR1000 after 50 h exposure to an air – 300 ppm SO_2 environment at 600 °C.

The two methods were shown to provide reasonable confidence in the results.

Following testing, both the stress-free and fatigue specimens were inspected using scanning electron microscopy and electron backscattered diffraction, EBSD (both using a Hitachi SU3500), whilst the fatigue specimens were also analysed using surface profilometry (Nanovea PS-50). The structure of oxide layers within corrosion pits and the underlying structure were identified using energy dispersive spectroscopy (EDS). In order to protect the absolute data, the results have been normalised with respect to the highest test stress used in the programme.

3. Results and discussion

3.1. Stress-free hot corrosion

The variation in metal loss data with salt composition for FG RR1000 at 600 °C; measured at 60 regularly spaced intervals around the bobbin circumference using an optical microscope, is plotted as a cumulative probability plot in Fig. 4. Given the relatively steep curves for all specimens, this indicates that there is little variation in pit size within each sample until approximately 90% cumulative probability. The distributions begin to plateau for the 10% exceedance data, which are arguably the most important for corrosion-fatigue lifing. Two samples per salting condition were prepared and give similar pit depth values and cumulative probability trends. The two sulphate-based salts; 98%Na_2SO_4-2% NaCl and 98%K_2SO_4-2%KCl resulted in similar cumulative probability

distributions up to 80% and produced greater maximum pit depths than the 55%K_2SO_4-45%KCl coated specimens. However, the 55%K_2SO_4-45%KCl (with a much larger proportion of chlorine) generally exhibits the most aggressive distribution until approximately 96% cumulative probability.

By considering the two samples as one dataset for each salt composition, the resultant average (mean) and maximum pit depths are shown in Fig. 5. The absolute maximum pit depth has been used, as under corrosion-fatigue conditions it would be expected that specimen failure would result in a crack developing from the largest pit, whilst the average pit depth of both data samples has also been used. As expected from the cumulative probability distribution (Fig. 4) the 98%K_2SO_4-2% KCl generated the largest maximum pit depth of 25.8 μm and second largest average pit depth of 4.7 μm. The second most damaging salt was 98%Na_2SO_4-2%NaCl, which has been commonly used in hot corrosion trials [3,14,15,23,24], with a maximum pit depth of 24.5 μm and average of 3.7 μm. Finally, 55%K_2SO_4-45%KCl produced the smallest maximum pitting damage, with a maximum pit depth of 18 μm despite having the largest average pit depth of 5.8 μm.

It is clear that even after a relatively short 50 h trial (typical stress free hot corrosion trials have previously lasted between 200 and 500 h [3]) the quantity of chloride had a greater effect on the hot corrosion behaviour of FG RR1000 than the choice of cation (potassium vs sodium). To date, work on type II hot corrosion of Ni-based alloys has typically investigated the effects of applying 98%Na_2SO_4-2%NaCl [14, 15,23,25–28], with several studies investigating pure Na_2SO_4 [29] and 80%Na_2SO_4-20%K_2SO_4 [24] at 700 °C. 700 °C has frequently been the chosen temperature for hot corrosion trials due to its link with the greatest corrosion rates under type II conditions as per the classic 'double-bell curve' [30]. The choice of 600 °C in this study allows the investigation of both lower temperature chloride-based mechanisms and type II hot corrosion (albeit not at the most damaging rate). Salt compositions with a molten eutectic at the desired test temperature have typically been used in corrosion trials due to the requirement for a liquid phase to induce the highest corrosion rates [31]. Previous work on the fireside corrosion of low-alloy steel at 550–600 °C [32] demonstrated that at 600 °C, the influence of a K_2SO_4-KCl eutectic on corrosion rates was greater than either pure KCl or K_2SO_4 at exposure lengths as short as 12 h. After only 50 h of hot corrosion in this study, the difference in maximum pitting damage between 55%K_2SO_4-45%KCl and 98% K_2SO_4-2%KCl was approximately 1.45x, ($\frac{25.8\mu m}{18\mu m}$ =1.43x). This compares well with the same low alloy steel study [32], that demonstrated a 1.65x increase in corrosion rates between pure K_2SO_4 and a K_2SO_4-KCl eutectic at 600 °C after 50 h of exposure ($\frac{4.85mg/cm^2}{2.9mg/cm^2}$ =1.67x (Interpolation of Fig. 14, [32])). In contrast there is not as stark a difference in pitting damage between 55%K_2SO_4-45%KCl and 98%Na_2SO_4-2%NaCl in this trial ($\frac{18\mu m}{24.5\mu m}$~ 0.74x) compared to previous work [22], which demonstrated that the influence of only a small quantity of chloride on hot corrosion damage at 600 °C on flat-plate FG RR1000 where the addition of 2%NaCl to pure Na_2SO_4 was shown to cause approximately twice the damage over the course of a 200-hour trial. However due to the salt application being more tightly controlled in this study, it is unsure if the significant increase in pitting was a result of greater salt flux or the difference in trial lengths (incubation versus propagation of hot corrosion).

3.2. Corrosion-fatigue

Due to the number of fatigue specimens available, it was decided to consider the effect of stress on the two most aggressive salts from previous work [22]; 55%K_2SO_4-45%KCl and 98%Na_2SO_4-2%NaCl. The selection of 98%Na_2SO_4-2%NaCl rather than 98%K_2SO_4-2%KCl for investigation allowed comparisons to be drawn with other studies at 700 °C [15]. Cyclic endurance lives for pre-salted FG material tested at 600 °C in a corrosive environment are shown in Fig. 6. The influence of shot-peening (or lack of in the stress-free trial) must also be considered; Gibson et al. [33] studied the influence of various shot-peening parameters on the type II hot corrosion of Ni-based superalloy alloy 720Li, which demonstrated that shot-peening increased the diffusion of sulphur into the bulk and reduced the adherence of protective chromium oxides due to the high angles of grain misorientation. However, shot peening also extends the fatigue lives of specimens by preventing crack initiation and is a commonly used surface treatment of gas turbine rotors. Therefore, in order to generate conditions representative of in-service rotors, it was necessary to shot peen the fatigue samples.

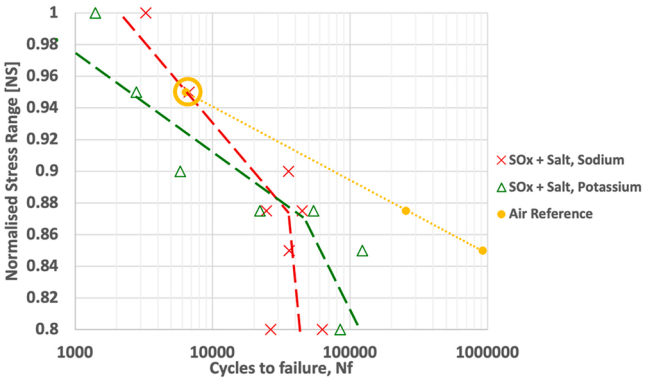

Fig. 6. Cyclic endurance lives of pre-salted material tested in a corrosive environment coated in 55%K_2SO_4-45%KCl (green triangles and dashed line) and 98%Na_2SO_4-2%NaCl (red crosses and dashed line) compared to an air-only reference (yellow dashed line) at 600 °C with an R-ratio of − 1. The yellow circle highlights the air-fatigue specimen which initiated from both surface and sub-surface initiation sites, thought to skew the air-fatigue best-fit line.

The cyclic endurance lives of pre-salted FG RR1000 tested in an air – 300 ppm SO_2 corrosive environment were compared to non-salted references, generated in air at 600 °C, Fig. 6. A portion of the S-N data was obtained from [22] with additional testing at lower stresses. It was observed that the application of salt resulted in the reduction of fatigue lives for a given applied stress. There appears to be a threshold normalised stress (NS) of 0.875, at which the two salt compositions exhibited similar lives and similar levels of variability. Above this threshold the increased chlorine content of 55%K_2SO_4-45%KCl significantly reduced the fatigue life of RR1000 compared to 98%Na_2SO_4-2% NaCl. A limited air-fatigue S-N dataset (three samples) was produced for comparison and highlights a larger difference in life from the corrosion-fatigue data at lower stresses, trending towards 98% Na_2SO_4-2%NaCl at high stresses. The air-fatigue specimen at 0.95 NS experienced crack growth from both surface and sub-surface initiation sites. Given the small sample size of the air-fatigue data, the sub-surface initiation and subsequent crack growth is thought to have artificially influenced the position of the air-fatigue best fit at higher stresses.

Fracture surfaces for the two salt compositions at the same applied stresses have been compared in Fig. 7. The samples had previously been cleaned with an Ardrox 1435b solution in an ultrasonic bath prior to surface profilometry, hence the lack of visible surface oxides. Counting of fatigue initiation sites on the fracture surfaces did not yield any significant differences between the two salt compositions at the given stress ranges that could offer an insight into the variability of fatigue lives (Table 1).

The S-N plot (Fig. 6) appears to show two distinct regions either side of a 0.875 NS threshold. Below an applied stress of 0.875 NS an almost vertical trend exists for the 98%Na_2SO4–2%NaCl coated fatigue specimens, whilst the 55%K_2SO_4-45%KCl coated specimens generally required a longer exposure time to the corrosive-fatigue environment before failure. In contrast, above the 0.875 NS threshold the increased chlorine content of the 55%K_2SO_4-45%KCl resulted in a significant reduction of fatigue lives. The two distinct regions will now be

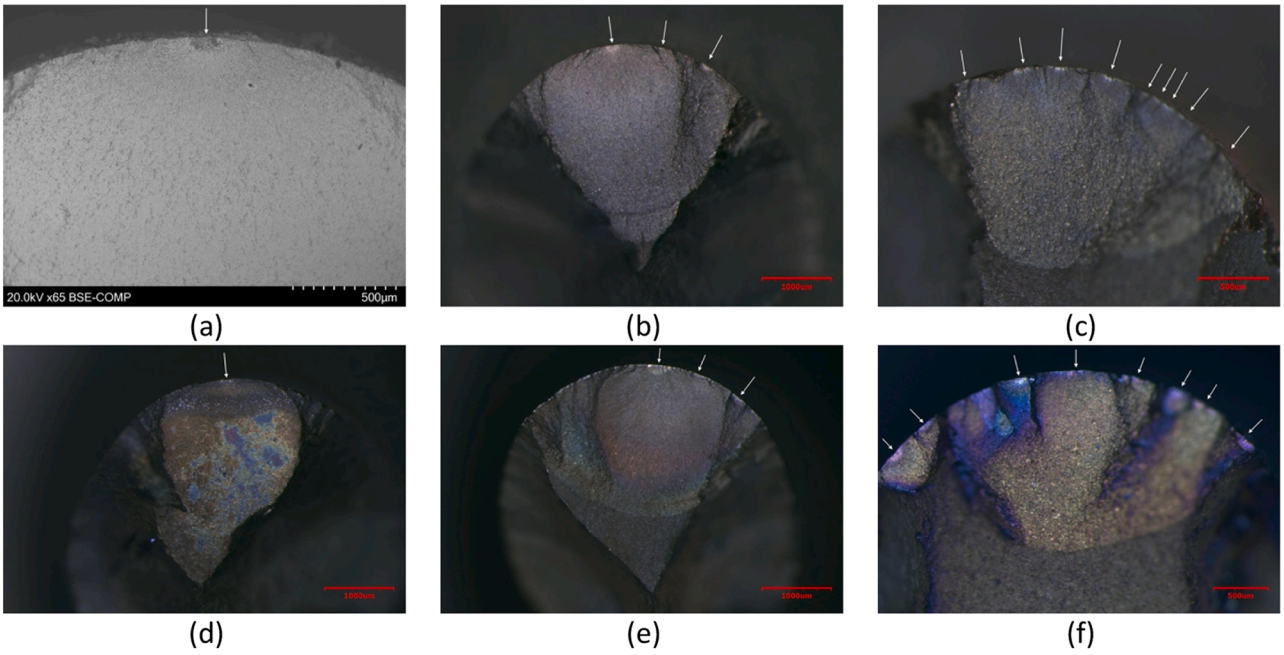

Fig. 7. Images of fracture surfaces for FG RR1000 coated with; (a)-(c) 55%K_2SO_4-45%KCl, (d)-(f) 98%Na_2SO_4-2%NaCl; at 0.80, 0.875 and 1.00 NS respectively. Note: (a) is a backscattered electron (BSE) image whilst the remainder were taken using an optical microscope.

Table 1
Number of crack initiation sites on the fracture surfaces of FG RR1000 fatigue specimens.

Salt Composition Applied Stress Range [NS]	55%K_2SO_4-45%KCl	98%Na_2SO4-2%NaCl
0.80	1	1
0.85	3	3
0.875	3	3
1.00	9	8

investigated and discussed separately.

3.3. Below 0.875 NS threshold

Below the threshold stress of 0.875 NS, the 98%Na_2SO_4-2%NaCl coated fatigue specimens failed between 26 and 62 K cycles (or 44–105 h of exposure based on the waveform used in this study). Generally, the 55%K_2SO_4-45%KCl required additional exposure lengths before failure. Whilst there is a degree of scatter within the fatigue specimens, it is not dissimilar to that experienced with similar Ni-based superalloys used in previous studies [15,26]. To assess the pit depths that may have led to crack initiation sites, surface profilometry of the gauge lengths of various specimens was conducted after oxide removal in an ultrasonic bath. This allowed a much greater area of the gauge

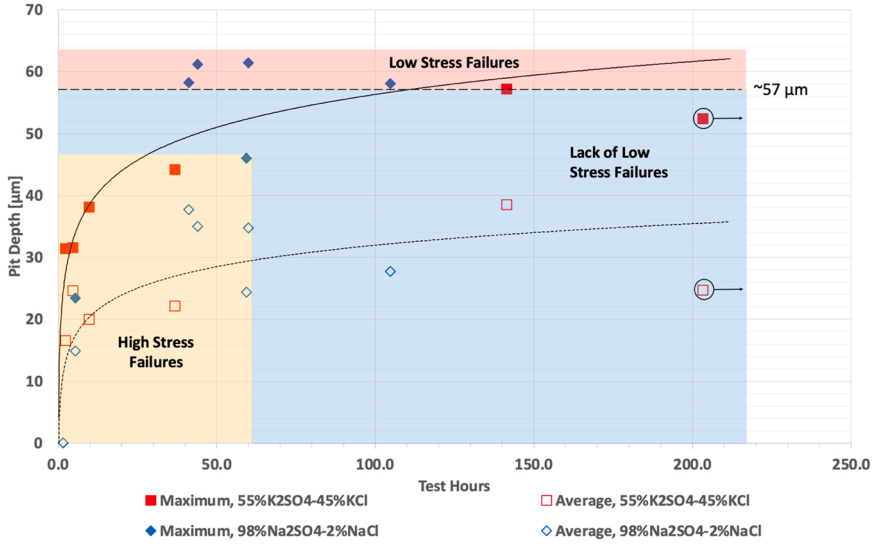

Fig. 8. Plot of maximum and average pit depths against the hours of exposure in an air – 300 ppm SO_2 environment at 600 °C. Trend lines have been plotted through the maximum (solid) and average (dotted) distributions for both salt compositions. Horizontal dashed line indicates the minimum metal loss required for a corrosion-fatigue specimen to fail below the 0.875 NS threshold. Arrowed circles indicate a specimen that was removed from test after 122,000 cycles/203 h without failure.

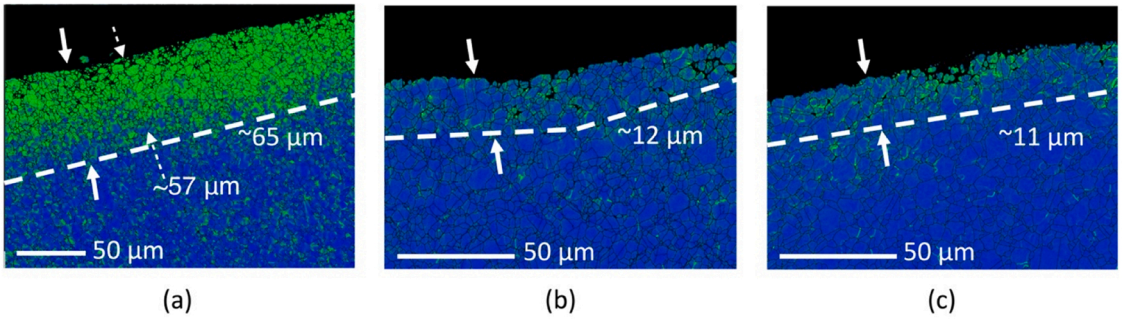

Fig. 9. EBSD local misorientation maps where 0° misorientation is represented by blue and 1.4° misorientation by green. (a) Left: Uncorroded, fatigue sample, shot-peened to 110H, 7–8 A, 200% conditions. Typical SHL depth of 65 µm. (b) Centre: Corroded fatigue sample, 0.875 NS, maximum pit depth of 44 µm, 12 µm of SHL remaining. (c) Right: Corroded fatigue sample, 0.90 NS, maximum pit depth of 38 µm, 11 µm of SHL remaining.

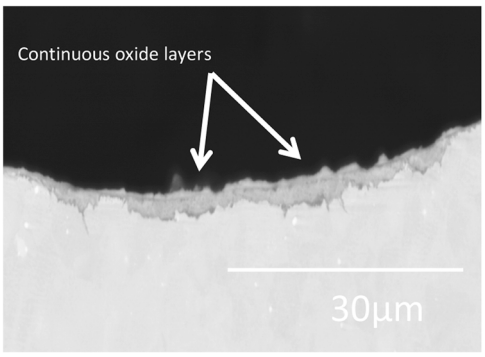

Fig. 10. Oxide structure of a 55%K_2SO_4-45%KCl coated fatigue specimen with an applied stress of 0.875 NS.

length to be analysed for pitting; thus, providing a more representative pit distribution than cross-sectioning and polishing to the mid-depth. However, it is acknowledged that this provides additional challenges using EDS to determine hot corrosion mechanisms. The oxide layers produced at 600 °C were significantly thinner than those produced at higher temperatures [3,15,24] and therefore any adherent scale is even less likely to influence the pit depths obtained through surface profilometry. The mean and maximum pit depths are presented in Fig. 8. The particular region of interest (i.e., below the 0.875 NS threshold) corresponds to an exposure length beyond 40 h, indicated by the red region in Fig. 8. It is observed that below this threshold stress the maximum pit depths (for failed specimens) all exceed 57 µm. A specimen coated in 55%K_2SO_4-45%KCl was removed from testing without failure after 122,000 cycles/203 h of corrosion-fatigue. Optical microscopy showed a maximum pit depth of 52 µm, below the minimum 57 µm of the failed specimens. Given that the fatigue specimens have been shot-peened, a strain hardened layer (SHL) has been introduced into the material surface. The current understanding [15] suggests that pitting of sufficient depth (i.e. beyond the SHL) is required before a dominant crack reaches long crack growth behaviour, eventually propagating to specimen failure. Therefore, EBSD local misorientation maps of pre-corroded and corroded fatigue specimens have been generated to determine the depth of SHL present, Fig. 9.

The local misorientation maps indicate that above the threshold, a SHL can still be observed. Therefore, the applied stress is sufficient to drive the crack growth behaviour and overcome the protective effects of the SHL. Whilst the typical depth of strain hardening has been approximated at 65 µm as per Fig. 9, the minimum and maximum depths can be seen to fluctuate either side of this typical depth. If the weakest link/shortest path is considered, then it may seem likely that long cracks will begin to form and propagate when corrosion damage has penetrated into less constrained material at these minimum depths of strain hardening. EBSD local misorientation maps were unable to be obtained for the low stress specimens due to resource availability. It is considered likely that the approximate minimum 57 µm of SHL observed in Fig. 9a is representative of the remaining corrosion-fatigue specimens, particularly when linked to the smallest maximum pit depths that caused failure below the threshold stress. The run-out of a specimen with only a maximum pit depth of 52 µm also supports the understanding that the SHL needs penetrating before a dominant fatigue crack can grow and propagate.

Examination of the oxide structure at 0.875 NS shows a continuous oxide formed on the alloy surface without any cracking (Fig. 10). It is interesting that at low stresses, the additional chlorine in the 55%K_2SO_4-45%KCl salt does not appear to have disrupted the surface oxides, given that the literature suggests that chlorine typically forms volatile chromium chlorides which act to disrupt protective oxides [34,35]. In fact, at these lower stresses, the relative proportion of sulphate appears to be the influencing factor rather than the chlorine. Stress-corrosion cracking studies of oil and gas pipeline steel [36] have shown that cracks typically initiated at corrosion pits. These pits were also found to nucleate from sulphide precipitates and inclusions in the material. Stress free type II hot corrosion does not typically involve the diffusion of sulphur into the base alloy [37], however previous work on RR1000 has shown sulphide diffusion at grain boundaries under low, relative stresses at 700 °C [16]. Given the relative proportions of sulphate in the two salts (98% vs 55% in 98%Na_2SO_4-2%NaCl and 55%K_2SO_4-45%KCl respectively) and their subsequent fatigue lives (shorter for 98%Na_2SO_4-2%NaCl under the proposed threshold stress of 0.875 NS), it is possible that greater sulphate proportions are more damaging at 600 °C under relatively low stresses. Recent work by Chan et al. [38,39] proposed that the formation of corrosion pits takes place once the solid eutectic $NiSO_4$-Na_2SO_4 approaches the eutectic composition and becomes molten. This work supports that proposal by demonstrating a reduction in pit initiation times for specimens with an increased quantity of Na_2SO_4/K_2SO_4. Thus the eutectic composition is reached sooner allowing the eutectic to melt and the formation of pits to occur more quickly.

Similar oxide structures have also been shown for FG RR1000 at 700 °C under low-stress corrosion fatigue conditions [15]. The authors proposed that where the applied stress was insufficient to generate fatigue cracking, a steady-state oxide scale is formed, leading to a lower impact on fatigue performance. This work supports that observation and proposal but would add that below the threshold stress of 0.875 NS, steady-state corrosion takes places until the SHL is sufficiently damaged, thus allowing a fatigue crack to grow. This has been suggested and achieved through sufficient pit depths at 700 °C [15] and 600 °C in this study.

High-magnification BSE images are presented for the two corrosion-fatigue samples subjected to the lowest stress, 0.80 NS, in Figs. 9 and 10. Sulphide diffusion along grain boundaries can be observed for both salting compositions to different extents. For the 55%K_2SO_4-45%KCl

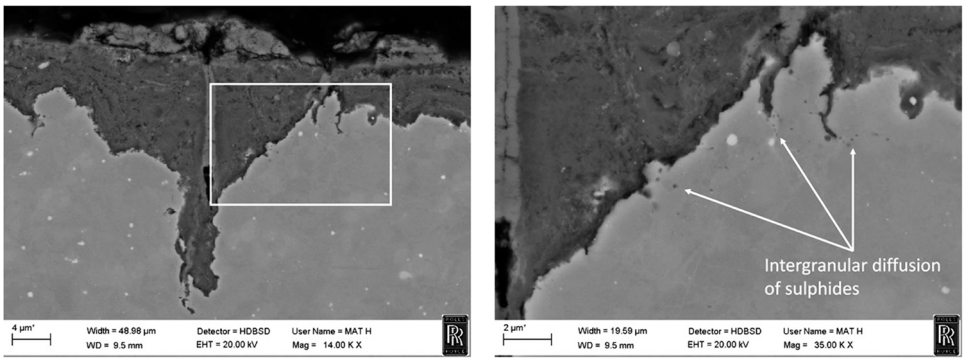

Fig. 11. (a) Left: High-magnification BSE image of a corrosion-fatigue specimen coated with 55%K_2SO_4-45%KCl subjected to 0.80 NS. (b) Right: Zoomed-in section showing intergranular diffusion of sulphides.

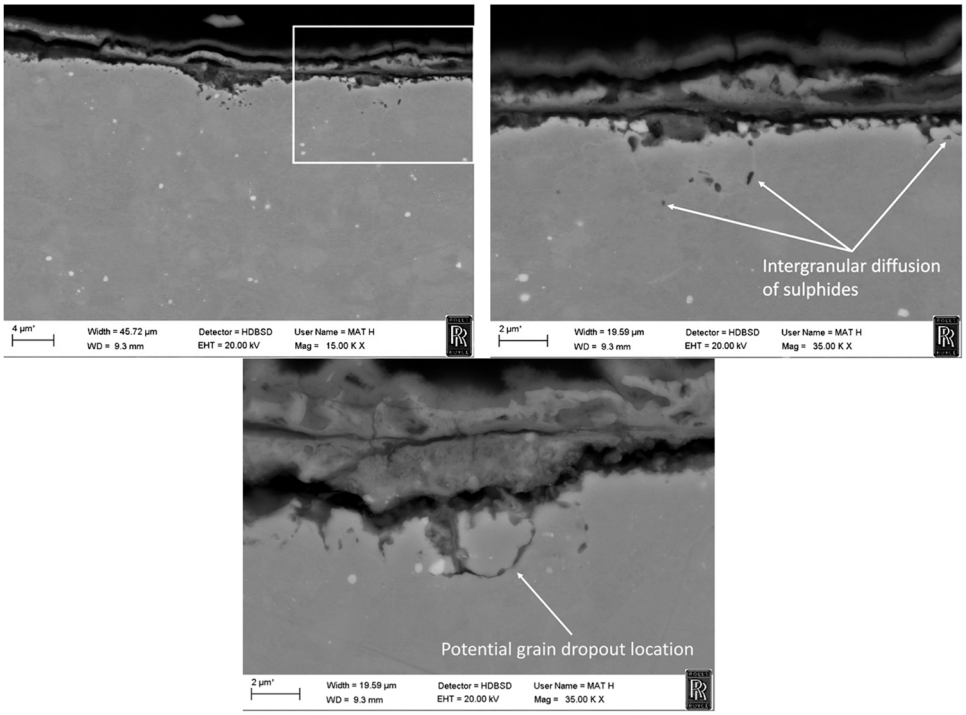

Fig. 12. (a) Top Left: High-magnification BSE image of a corrosion-fatigue specimen coated with 98%Na_2SO_4-2%NaCl subjected to 0.80 NS. (b) Top Right: Zoomed-in section showing intergranular diffusion of sulphides. Bottom Centre: Zoomed-in section at a different location of the gauge length showing severe weakening of a grain boundary.

coated specimen (Fig. 11), sulphide diffusion was typically constrained within larger features and less prevalent along the gauge length. Whereas the 98%Na_2SO_4-2%NaCl coated specimen (Fig. 12) exhibited sulphide ingress ahead of the corrosion front frequently along the gauge. It was observed that at one location, the sulphide diffusion had sufficiently weakened the boundaries of a grain leading to the early stages of grain dropout. It is thought that the increased prevalence of sulphide diffusion and penetration ahead of the corrosion front is due to the relative sulphate composition of the salt and assists with penetrating the SHL sooner than the equivalent 55%K_2SO_4-45%KCl coated counterpart.

During early stages of the study, whilst determining the location of the S-N distribution at 600 °C, a one-off fatigue test was setup at 0.65 NS and removed from test after 285 K cycles (475 h of SO_2 exposure) without failure. The specimen was not cleaned and was mounted in Bakelite with the oxide intact. The resultant cross-section and EDS maps are shown in Fig. 13. Type II hot corrosion is typically characterised by the formation of protective aluminium and chromium oxides adjacent to the alloy with gradual diffusion of sulphur into the alloy-oxide interface and the outermost oxides comprise of nickel and cobalt in a non-protective layer. The EDS imagery provides good confidence that type II hot corrosion has been replicated in this study at the lower temperature of 600 °C in FG RR1000. Additionally, the lack of cracks in the oxide layer suggests that the corrosion continues in a steady-state manner well below the 0.875 NS threshold, even for significant exposure lengths.

3.4. *Above 0.875 NS threshold*

Above the threshold stress, there is a clear influence of salt composition on the resultant fatigue lives. Examination of the oxide structures (Fig. 14) and fracture surfaces (Fig. 7) shows that at high stresses there is minimal corrosion product or pitting on the specimen surface, resulting in a minimal reduction in fatigue life when compared to air-fatigue. At high stress-ranges, fatigue mechanisms are the "weakest link" and

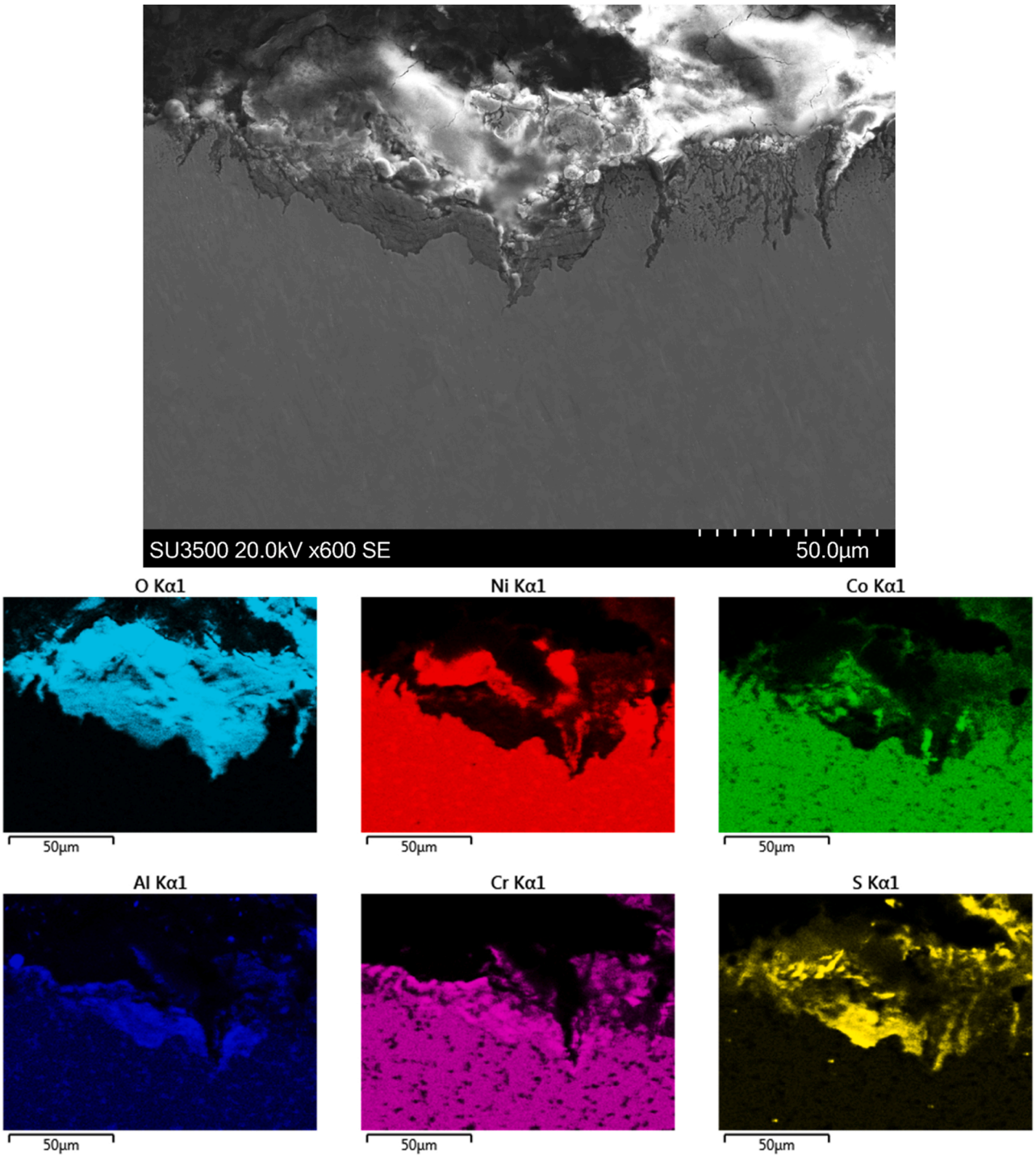

Fig. 13. SEM and EDS images of a 55%K_2SO_4-45%KCl coated specimen subjected to corrosion-fatigue at 0.65 NS for 475 h.

therefore there is often insufficient time for corrosion mechanisms to propagate (Fig. 14a). The most interesting feature of Fig. 14 is the apparent increase in corrosion damage at intermediate stress ranges (0.90–0.95 NS, Fig. 14b,c). The formation of stress raising features can be seen in as few as 5 h, surrounded by broken oxide scale. As the applied stress is further reduced (Fig. 10, Fig. 13), the oxide layer appears to be stable and is frequently continuous with no secondary fissure formation across the gauge length. Localised pitting can be seen to occur at low stress-ranges compared to crack formation at high stress-ranges. The number of fissures exceeding a threshold length of 10 µm is given in Table 2.

The generation of a greater number of cracks at high stresses is thought to allow chlorine to diffuse more readily into the alloy, promoting enhanced crack growth rates. Analysis of striation counts was conducted in order to provide a useful approximation of the crack growth rates. An example image of a fatigue sample fracture surface shows where striation counts were taken and subsequently averaged for a crack length of the image midpoint (Fig. 15). The approximate stress intensity factor, K, was calculated for each averaged striation count using Equation 1 [40]. The average crack growth rate, da/dN, for each image was measured and calculated at the midpoint of each image, giving a matching datapoint for the estimated stress intensity factor.

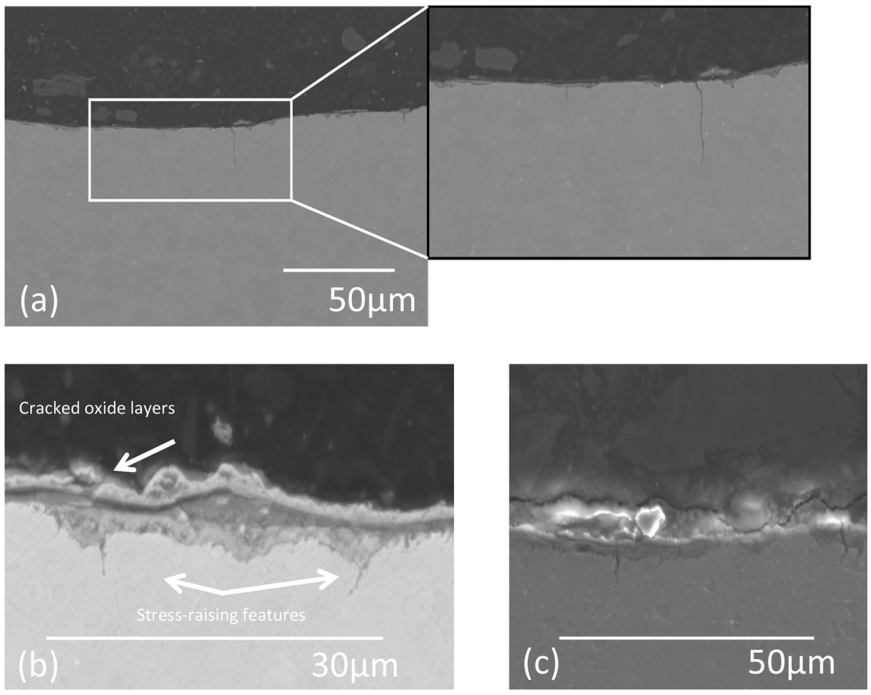

Fig. 14. (a) Example of high stress corrosion-fatigue conditions, displaying minimal surface corrosion product and cracking of the alloy. Stress-range of 1.00 NS; (b) Example of oxide formation at intermediate stress-ranges. Stress-range of 0.95 NS; (c) Example of lower intermediate stress corrosion-fatigue conditions. Stress-range of 0.90 NS.

Table 2
Number of fissure lengths exceeding 10 µm for corrosion-fatigue specimens coated with 55%K_2SO_4-45%KCl.

Normalised Stress-Range [NS]	55%K_2SO_4-45%KCl		98%Na_2SO_4-2%NaCl	
	Length of SO_2 exposure [h]	Number of fissures > 10 µm	Length of SO_2 exposure [h]	Number of fissures > 10 µm
1.00	2.3	12	5.4	3
0.95	4.6	8	11.2	2
0.90	9.7	1	59.4	9
0.875	36.8	0	41.1	3

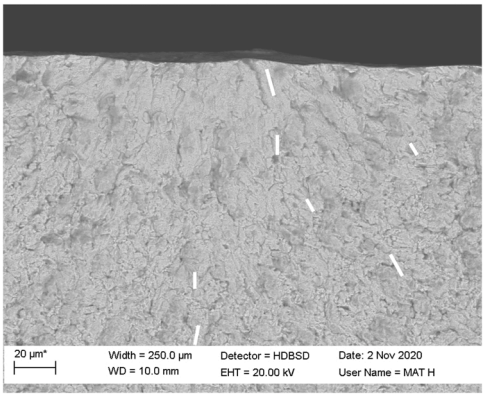

Fig. 15. BSE image of an initiation site on the fatigue sample subjected to 0.95 NS coated with 98%Na_2SO_4-2%NaCl. The annotated white lines indicate where striation counting was conducted.

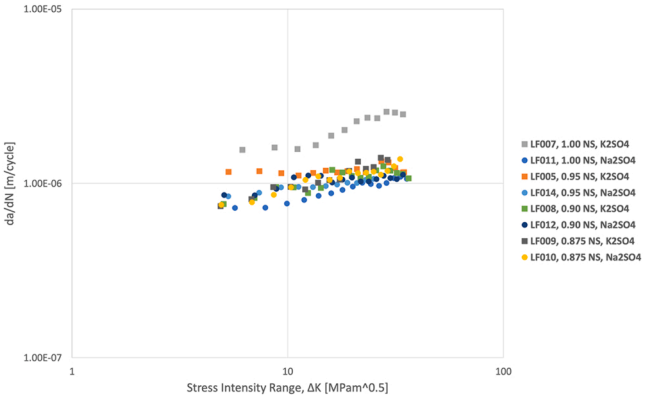

Fig. 16. Striation measured crack growth rates for 55%K_2SO_4-45%KCl (square markers) and 98%Na_2SO_4-2%NaCl (circular markers) coated specimens.

Equation 1 Estimation of stress intensity factor [40].

$$K = Y\sigma\sqrt{\pi a}$$

where;

$$Y = G(0.752 + 1.286\beta + 0.37H^3)$$

$$G = 0.92\left(\frac{2}{\pi}\right)\sec\beta\sqrt{\frac{\tan\beta}{\beta}}$$

$$H = 1 - \beta$$

$$\beta = \frac{\pi}{2}\frac{a}{diameter}$$

The resultant estimated crack growth rates (Fig. 16) show that the crack growth rates are similar for the 98%Na_2SO_4-2%NaCl coated specimens at all applied stress ranges. This can also be said for the 55%

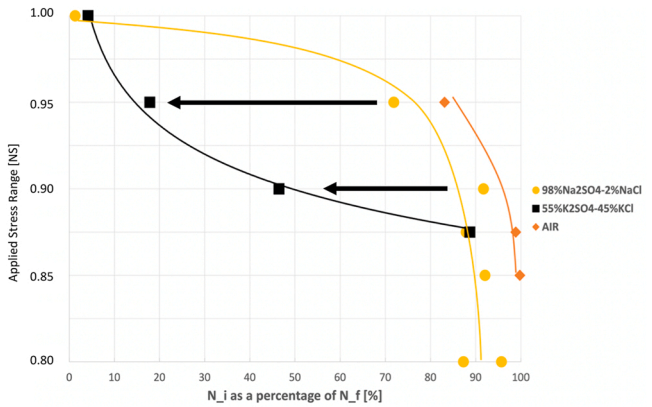

Fig. 17. Estimates of $N_{initiation}$ as a percentage of $N_{failure}$ for FG RR1000 fatigue specimens coated in 55%K_2SO_4-45%KCl and 98%Na_2SO_4-2%NaCl subjected to an air-300 ppm SO_2 environment at 600 °C. A limited dataset of air-only fatigue specimens is shown for comparison. Arrows depict the reduction of time/cycles required to initiate a fatigue crack at 0.90 and 0.95 NS.

K_2SO_4-45%KCl coated specimens at and below 0.90 NS. Interestingly, the crack growth rates of 55%K_2SO_4-45%KCl are greater initially for both 0.95 and 1.00 NS, and clearly higher for 1.00 NS across the entire stress intensity range. Having measured the fatigue striations on the fracture surface, predictions of the number of cycles required to initiate a fatigue crack can be made using:

$$N_{failure} = N_{initiation} + N_{propagation}$$

Given that $N_{failure}$ is known from the S-N curve and $N_{propagation}$ has been estimated through the striation counts, $N_{initiation}$ can be determined. The percentage of cycles required to initiate a fatigue crack for the two salt compositions and air-only, at stress ranges of 0.80–1.00 NS are shown in Fig. 17. It is clear that at 0.90 and 0.95 NS, the specimens coated in 55%K_2SO_4-45%KCl experienced a significant reduction in the time/number of cycles required to initiate a crack. This reduction of crack initiation from the air-only baseline is much greater for the 55% K_2SO_4-45%KCl (79%) compared to that exhibited by the 98%Na_2SO_4-2%NaCl (15%). Chlorine induced hot corrosion is thought to be the result of chlorine production via oxychlorination [41]. The NaCl acts as a catalyst of the reaction between the alloy and oxygen, thereby accelerating the rate of corrosion. Highly volatile Na_2CrO_4 and $CrCl_2$ form which create voids and pits at grain boundaries and facilitate the movement of damaging species with oxygen [34,35]. The high penetration power of small chlorine ions is associated with this adverse effect by influencing the initial protective oxide formation [35]. Pure NaCl has previously been shown to be aggressive at both 550 °C and 650 °C despite having a melting temperature (T_m = 801 °C) significantly above the test temperatures [34]. The increased chlorine content of the salt has reduced fatigue lives and initiation time in only a narrow stress band, between 0.875 and 1.0 NS. The application of a stress sufficient to cause oxide cracking (as seen in Fig. 14b,c) suggests the possibility of protective oxide disruption, exacerbated by volatile chloride ingress. Whilst there was little apparent difference in the number of initiation sites on the fracture surface for the two salt compositions, fissure counts (Table 2) on the sample cross-sections showed 4x as many fissures exceeding 10 μm for the 55%K_2SO_4-45%KCl coated specimens at these higher stresses. The use of $N_{initiation}$ as a percentage of $N_{failure}$ removes the effect of the different fatigue lifetimes when comparing the two salt compositions. At 0.90 NS, the increased chlorine resulted in a 49% reduction of $N_{initiation}$. Likewise at 0.95 NS the reduction of $N_{initiation}$ was even greater at 61%. It is thought that the two salt compositions converge back together at 1.00 NS as this is very close to the yield strength of the material. It would be expected that at the yield strength, that damage is being introduced from the first complete fatigue cycle.

Therefore, it is proposed that increased chlorine content results in reduced fatigue lifetimes above a threshold stress of 0.875 NS. This is achieved through a reduction in time required for fatigue crack initiation and initiation at additional sites (0.90 and 0.95 NS). Future experimental work should include the use of oil-based polishing compounds and media, to allow investigation into the presence of chlorine at crack tips via EDS.

4. Conclusions

A series of type II hot corrosion exposures have been carried out on the FG variant of Ni-based superalloy, RR1000. The effect of salt composition has been shown to have an effect on type II hot corrosion at 600 °C, particularly at intermediate to high stresses for corrosion-fatigue conditions. Chlorine is thought to influence the fatigue lives of RR1000 at 600 °C above a threshold stress by reducing the time required for fatigue crack initiation at intermediate – high stresses and by producing additional initiation sites. It is postulated that at these high stresses, the mechanical cracking of the surface oxide scales allows easier and additional diffusion pathways to the parent alloy for the chlorine. Below this threshold, stresses are not sufficient to generate cracking of the oxide scales or alloy and therefore allow chlorine ingress. Therefore, it is proposed that steady-state corrosion and sulphide diffusion will take place until the strain-hardened layer has been penetrated, thus allowing a fatigue crack to form. At these lower stresses, the relative proportion of sulphate rather than chloride has been shown to be more influential of fatigue life.

CRediT authorship contribution statement

M.L. Hendery: Conceptualization, Methodology, Validation, Formal analysis, Investigation, Data curation, Writing – original draft, Writing – review & editing, Visualization, Project administration. **M.T. Whittaker:** Conceptualization, Resources, Writing – original draft, Writing – review & editing, Supervision, Project administration, Funding acquisition. **B.J. Cockings:** Conceptualization, Methodology, Validation, Investigation, Data curation, Writing – original draft, Writing – review & editing, Supervision. **P.M. Mignanelli:** Conceptualization, Resources, Writing – review & editing, Supervision, Funding acquisition.

Declaration of Competing Interest

The authors declare that they have no known competing financial interests or personal relationships that could have appeared to influence the work reported in this paper.

Data Availability

The raw/processed data required to reproduce these findings cannot be shared at this time due to legal reasons

Acknowledgements

The current research was funded by the EPSRC Rolls-Royce Strategic Partnership in Structural Metallic Systems for Gas Turbines (grants EP/H500383/1 and EP/H022309/1) alongside the Materials and Manufacturing Academy (M2A) supported through the European Social Fund. The provision of materials and supporting information from Rolls-Royce plc is gratefully acknowledged. Mechanical testing was performed by MLH and BJC at Swansea Materials Research and Testing Ltd. (SMaRT).

References

[1] T.M. Pollock, S. Tin, Nickel-based superalloys for advanced turbine engines: chemistry, microstructure, and properties, J. Propuls. Power 22 (2006) 361–374.

[2] M. Darecki, C. Edelstenne, T. Enders, E. Fernandez, P. Hartman, J.-P. Herteman, M. Kerkloh, I. King, P. Ky, M. Mathieu, G. Orsi, G. Schotman, C. Smith, J.-D. Wörner, Flightpath 2050 (2011), https://doi.org/10.2777/50266.

[3] A. Encinas-Oropesa, G.L. Drew, M.C. Hardy, A.J. Leggett, J.R. Nicholls, N.J. Simms, Effects of oxidation and hot corrosion in a nickel disc alloy, in: Proceedings of Superalloys 2008 11th Int. Symp. Superalloys, 2008, pp. 609–618. ⟨https://doi.org/10.7449/2008/Superalloys_2008_609_618⟩.

[4] H.T. Corrosion, Hot corrosion in gas turbines, High Temp. Corros. Mater. Appl. (2007) 249–258, https://doi.org/10.1361/hcma2007p249.

[5] J.A. Goebel, F.S. Pettit, Na2SO4-induced accelerated oxidation (Hot Corrosion) of nickel, Metall. Trans. 1 (1970) 1943–1954.

[6] J.K. Tien, T. Caulfield, Superalloys, supercomposites and superceramics, (n.d.).

[7] K.L. Luthra, O.H. LeBlanc, Low temperature hot corrosion of Co-Cr-Al Alloys, Mater. Sci. Eng. 87 (1987) 329–335, https://doi.org/10.1016/0025-5416(87)90395-8.

[8] J. Pettersson, N. Folkeson, L.G. Johansson, J.E. Svensson, The effects of KCl, K 2SO 4 and K 2CO 3 on the high temperature corrosion of a 304-type austenitic stainless steel, Oxid. Met. 76 (2011) 93–109, https://doi.org/10.1007/s11085-011-9240-z.

[9] G. Salinas-Solano, J. Porcayo-Calderon, J.G. Gonzalez-Rodriguez, V.M. Salinas-Bravo, J.A. Ascencio-Gutierrez, L. Martinez-Gomez, High temperature corrosion of inconel 600 in NaCl-KCl molten salts, Adv. Mater. Sci. Eng. 2014 (2014) 1–8, https://doi.org/10.1155/2014/696081.

[10] J. He, W. Xiong, W. Zhang, W. Li, K. Long, Study on the high-temperature corrosion behavior of superheater steels of biomass-fired boiler in molten alkali salts' mixtures, Adv. Mech. Eng. 8 (2016) 1–9, https://doi.org/10.1177/1687814016678163.

[11] T.P. Gabb, J. Telesman, B. Hazel, D.P. Mourer, The effects of hot corrosion pits on the fatigue resistance of a disk superalloy, 2009. ⟨https://doi.org/10.1007/s11665-009-9399-5⟩.

[12] J.K. Sahu, R.K. Gupta, J. Swaminathan, N. Paulose, S.L. Mannan, Influence of hot corrosion on low cycle fatigue behavior of nickel base superalloy SU 263, Int. J. Fatigue 51 (2013) 68–73, https://doi.org/10.1016/j.ijfatigue.2013.02.006.

[13] J. Telesman, T.P. Gabb, Y. Yamada, S.L. Draper, Fatigue resistance of a hot corrosion exposed disk superalloy at varied test temperatures, Mater. High Temp. 33 (2016) 517–527, https://doi.org/10.1080/09603409.2016.1179000.

[14] M. Dowd, K.M. Perkins, D.J. Child, Pre-notched and corroded low cycle fatigue behaviour of a nickel-based alloy for disc rotor applications, Int. J. Fatigue 105 (2017) 7–15, https://doi.org/10.1016/j.ijfatigue.2017.08.009.

[15] D.J. Child, J. Meldrum, P. Onwuarolu, Corrosion-fatigue testing of Ni-based superalloy RR1000, Mater. Sci. Technol. 33 (2017) 1040–1047, https://doi.org/10.1080/02670836.2016.1242827.

[16] H.L. Cockings, K.M. Perkins, M. Dowd, Influence of environmental factors on the corrosion-fatigue response of a nickel-based superalloy, Mater. Sci. Technol. 33 (2017) 1048–1055, https://doi.org/10.1080/02670836.2017.1300419.

[17] S. Pedrazzini, D.J. Child, T. Aarholt, C. Ball, M. Dowd, A. Girling, H. Cockings, K. Perkins, M.C. Hardy, H.J. Stone, P.A.J. Bagot, On the effect of environmental exposure on dwell fatigue performance of a fine-grained nickel-based superalloy, Metall. Mater. Trans. A Phys. Metall. Mater. Sci. 49 (2018) 3908–3922, https://doi.org/10.1007/s11661-018-4752-7.

[18] M.C. Hardy, B. Zirbel, G. Shen, R. Shankar, Developing damage tolerance and creep resistance in a high strength nickel alloy for disc applications, Superalloys 2004 (2004) 83–90.

[19] R.C. Reed, Superalloys: Fundam. Appl. (2015), https://doi.org/10.1017/CBO9781107415324.004.

[20] H. Rosier, M. Dowd, K. Perkins, G. Gibson, Development and Validation of an Automated Salt Spray Procedure for SILOET II WP 17.2.4.1, 2015.

[21] H.L. Cockings, K. Perkins, S. Gray, Optimisation of a salt deposition technique for the corrosion-fatigue testing of nickel based superalloys, Mater. High Temp. 35 (2018) 451–460, https://doi.org/10.1080/09603409.2017.1380943.

[22] M.L. Hendery, M.T. Whittaker, B.J. Cockings, P.M. Mignanelli, The Effect of Salt Chemistry on the Zero and Cyclic Load Performance of a High Temperature Nickel-Based Superalloy, in: Proc. 8th E[1] M.L. Hendery, M.T. Whittaker, B.J. Cockings, P.M. Mignanelli, Eff. Salt Chem. Zero Cycl. Load Perform. a High Temp. Nickel-Based Superalloy, Proc. 8th Eng. Integr. Soc. Int. Conf. Durab., Engineering Integrity Society, Cambridge, 2021.

[23] T. Gheno, B. Gleeson, On the hot corrosion of nickel at 700 °C, Oxid. Met. 84 (2015) 567–584, https://doi.org/10.1007/s11085-015-9588-6.

[24] J. Sumner, A. Encinas-Oropesa, N.J. Simms, J.R. Nicholls, Type II hot corrosion: kinetics studies of CMSX-4, Oxid. Met. 80 (2013) 553–563, https://doi.org/10.1007/s11085-013-9395-x.

[25] H.L. Cockings, B.J. Cockings, W. Harrison, M. Dowd, K.M. Perkins, M.T. Whittaker, G.J. Gibson, The effect of near-surface plastic deformation on the hot corrosion and high temperature corrosion-fatigue response of a nickel-based superalloy, J. Alloy. Compd. 832 (2020), 154889, https://doi.org/10.1016/j.jallcom.2020.154889.

[26] H.L. Rosier, Role of the Environment and its Effects on the High Temperature Corrosion-Fatigue Life in Nickel Based Superalloys, n.d.

[27] J.R. Nicholls, N.J. Simms, A. Encinas-Oropesa, Modelling hot corrosion in industrial gas turbines, Mater. High Temp. 24 (2007) 149–162, https://doi.org/10.3184/096034007×263587.

[28] J. Sumner, A. Encinas-Oropesa, N.J. Simms, J.R. Nicholls, Type II hot corrosion: behavior of CMSX-4 and IN738LC as a function of corrosion environment, Mater. Corros. 65 (2014) 188–196, https://doi.org/10.1002/maco.201307425.

[29] T. Gheno, B. Gleeson, On the hot corrosion of nickel at 700 °C, Oxid. Met. 84 (2015) 567–584, https://doi.org/10.1007/s11085-015-9588-6.

[30] D.E.J. Talbot, J.D.R. Talbot. Corrosion Science and Technology, Second ed., CRC Press, 2007. ⟨https://books.google.co.uk/books?id=MxPNBQAAQBAJ⟩.

[31] K.L. Luthra, D.A. Shores, Mechanism of Na2SO4 induced corrosion at 600–900 °C, J. Electrochem. Soc. 127 (1980) 2202–2210.

[32] A. Mlonka-Mędrala, K. Gołombek, P. Buk, E. Cieślik, W. Nowak, The influence of KCl on biomass ash melting behaviour and high-temperature corrosion of low-alloy steel, Energy 188 (2019), 116062, https://doi.org/10.1016/j.energy.2019.116062.

[33] G.J. Gibson, K.M. Perkins, S. Gray, A.J. Leggett, Influence of shot peening on high-temperature corrosion and corrosion-fatigue of nickel based superalloy 720Li, Mater. High Temp. 33 (2016) 225–233, https://doi.org/10.1080/09603409.2016.1161945.

[34] G.S. Mahobia, N. Paulose, V. Singh, Hot corrosion behavior of superalloy IN718 at 550 and 650°C, J. Mater. Eng. Perform. 22 (2013) 2418–2435, https://doi.org/10.1007/s11665-013-0532-0.

[35] D. Pradhan, G. Shankar Mahobia, K. Chattopadhyay, V. Singh, Salt induced corrosion behaviour of superalloy IN718, Mater. Today Proc. 5 (2018) 7047–7054, https://doi.org/10.1016/j.matpr.2017.11.368.

[36] M. Elboujdaini, R.W. Revie, Metallurgical factors in stress corrosion cracking (SCC) and hydrogen-induced cracking (HIC), J. Solid State Electrochem. 13 (2009) 1091–1099, https://doi.org/10.1007/s10008-009-0799-0.

[37] J. Stringer, High-temperature corrosion of superalloys, Mater. Sci. Technol. 3 (1986) 482–493, https://doi.org/10.1080/02670836.1987.11782259.

[38] K.S. Chan, M.P. Enright, J. Moody, C. Thomas, W. Goodrum, HOTPITS: The DARWIN approach to assessing risk of hot corrosion-induced fracture in gas turbine components, Eng. Fract. Mech. 228 (2020), 106889, https://doi.org/10.1016/j.engfracmech.2020.106889.

[39] K.S. Chan, M.P. Enright, J.P. Moody, S.H.K. Fitch, Physics-based modelling tools for predicting type II hot corrosion in nickel-based superalloys, in: M. Hardy, E. Huron, U. Glatzel, B. Griffin, B. Lewis, C. Rae, V. Seetharaman, S. Tin (Eds.), Superalloys 2016 Proc. 13th Int. Symp. Superalloys, TMS, 2016: pp. 917–925.

[40] H.A. Wood, R.M. Engle, USAF damage tolerant design handbook: guidelines for the analysis and design of damage tolerant aircraft structures, Tech. Rep. AFFDL-TR - Air Force Flight Dyn. Lab. 16 (1979).

[41] T.S. Sidhu, A. Malik, S. Prakash, R.D. Agrawal, Cyclic oxidation behavior of ni- and fe-based superalloys in air and Na2SO4-25%NaCl molten salt environment at 800°C, Int. J. Phys. Sci. 1 (2006) 27–33.